Materials, experimental design, and characterization methods

2.1: Materials

2.1.1: Pluronic® Polymers

The triblock copolymers with a class of PEO-PPO-PEO, which are available commercially as Pluronic® or Lutrol® ("Poloxamers"--non-commercial name), provide a series of more than 50 polymeric surfactants with a wider range of molecular weights, from as high as 14600 for L108 to as low as 1630 for L42.

Pluronics are approved by the U.S. FDA. They are widely used for drug solubilization and their specific delivery, as well as in gene delivery, diagnostics, and tissue engineering. It is because they are non-ionic, non-toxic, can form micelles, and are biocompatible and biodegradable.

The Pluronic polymers used in the thesis work are shown in Table 2.1 with their general characteristics.

- Three important Pluronic polymers (F127, P123 and F68) were obtained from Sigma-Aldrich (St.Luice, MO, USA) and used as received.
- Pluronic F88 was received as gift sample from BASF Corporation (USA).

Table 2.1: Molecular properties of studied Pluronics.

Pluronic®	Mol.Wt. ($g.mol^{-1}$)	nEO	nPO	CPT(°C) @ %w/v	CMC$ (%w/v)	HLB	CMC$ (%w/v)	CMT (°C)
F127	12600	100	65	>100°	0.02 *	22	0.02 *	24°
F88	11400	104	48	>100°	1.7 #	28	1.7 #	38°
F68	8400	76	29	>100°	7.0#	>24	7.0#	50°
P123	5800	20	70	90°	0.001*	8	0.001*	16°

#@high temperature (>30°C), *@room temperature (30°C), $ @taken from references [1,2].

2.1.2: Biocompatible materials

2.1.2.1: L-α-Phosphatidylcholine

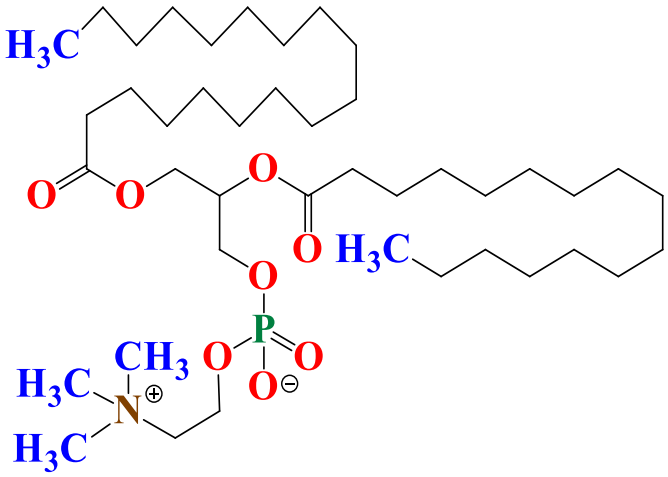

Figure 2.1: Molecular structure of PC.

PC, a naturally occurring phospholipid, is a nontoxic and biocompatible material that has been used by food and pharmaceutical companies. The compatibility of the PC with human membranes and skin is the first and most important advantage of a PC-based vesicular system. Hence, PC based formulations improve the therapeutic efficacy of lipophilic drugs. PC provide distinct benefits for a surface-active component because they are nontoxic, well-tolerated parenterally, and have excellent biocompatibility [3,4].

The general properties of PC are shown in Table 2.2.

- The PC for investigations was purchased from Alfa Aesar (part of Thermo Fisher Scientific (India)) and used as received after proper checking and analysis of the properties given by the supplier.

Table.2.2: General properties of PC

Physical state	Light yellow Powder
Molecular formula	$C_{44}H_{88}NO_8P$
Molecular weight (g mol^{-1})	786.1
Melting Point	236ºC

2.1.2.2: D-α-Tocopherol polyethylene glycol 1000 succinate

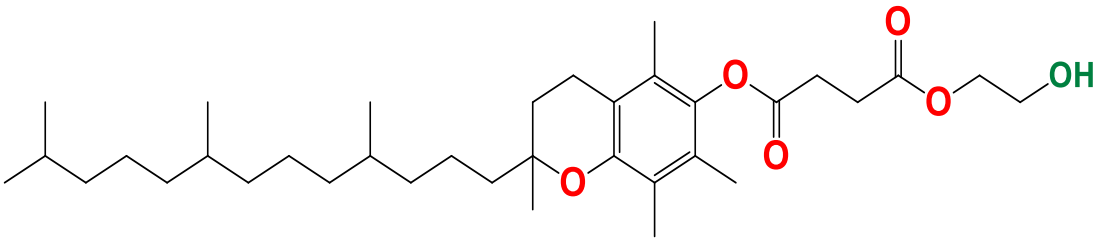

Figure 2.2: Molecular structure of TPGS

TPGS (Figure 2.2) is a nonionic amphiphile formed by the esterification of vitamin E succinate. The US-FDA and EMA have classified it as a safe excipient. TPGS, like other PEG condensates, spontaneously forms kinetically stable core-shell micelles (diameter 12-15 nm) and has interesting properties as a emulsifier, solubilizer, gelling agent and dispersant. Its aggregation behavior can be modified by combining it with other amphiphilic materials and organic additives. These characteristic have been used to developed a wide range of vesicular, semisolid, and multiparticulate pharmaceuticals. It increases drug bioavailability by increasing permeation and decreasing P-glycoprotein levels.

TPGS has undergone testing to create various drug formulations, including micelles, microemulsions, vesicles, and nanoparticles. TPGS surface modification of solid and polymeric lipid nanoparticles enhances transcellular drug uptake, prolongs blood circulation time, and improves drug encapsulation effectiveness [5,6].

The general properties of TPGS are shown in Table 2.3

- TPGS was gift sample from Connell Bros. Company Private Limited (Mumbai, India)

Table.2.3: General properties of TPGS

Physical state	White Waxy solid
Molecular formula	$C_{35}H_{58}O_6$
Molecular weight (g.mol^{-1})	~1513
CMC$^{\$}$ (%w/v)	0.02
Melting Point (°C)	38ºC

$^{\$}$ reported from ref.[6]

2.1.2.3: Stearic Acid (SA)

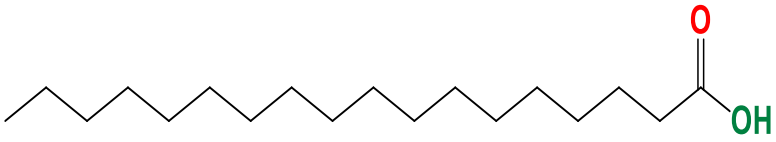

Figure 2.3: Molecular structure of Stearic acid

SA (Figure 2.3), also known as octadecanoic acid, is derived from fats and oils derived from animals and plants. SA can be synthesized by humans. SA is an 18-carbon chain saturated fatty acid that is commonly used in food preparation, softening agents, and release agents [7].

The general properties of SA are shown in Table 2.4

- SA was procured from ThermoFisher Scientific™ (Mumbai, India)

Table.2.4: General properties of SA

Physical state	White powder
Molecular formula	$C_{18}H_{36}O_2$
Form	Crystal or Powder
Molecular weight (g mol^{-1})	284.48
Melting Point	67ºC

2.1.3: Lipophilic Drugs

2.1.3.1: Quercetin

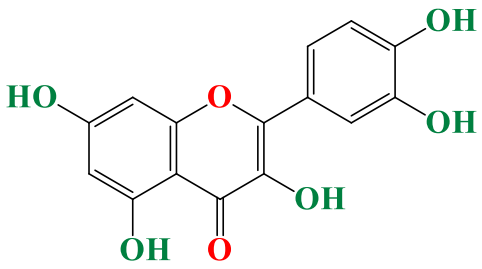

Figure 2.4: Molecular structure of Quercetin

QCN is a bioactive flavonoid that is in the glands located on the surface of leaves, flowers, or fruits of plants. Chemically, QCN consists of three aromatic rings with five hydroxyl groups, where the two rings I and II, are linked by oxygen-containing six-member heterocyclic ring III (shown in Figure 2.4). QCN has a wide spectrum of pharmacological and biological properties, including anti-carcinogenic, anti-diabetic, antiulcer, anti-inflammatory, antiviral, and anti-allergic effects. As apotent antioxidant scavenges free radicals directly inhibits xanthine oxidase, alters antioxidant defence, and inhibits lipid peroxidation [8,9]. However, the application of QCN has been limited as a therapeutic molecule due to poor oral bioavailability because of low aqueous solubility. With low solubility, QCN shows the shortcomings of poor permeability, instability in physiological medium, short biological half-life, extensive first past metabolism before reaching systemic circulation [10,11].

The general properties of QCN are shown in Table 2.5.

- QCN were procured from Sigma-Aldrich (St.Luice, MO, USA).

Table.2.5: General properties of QCN

Physical state	Solid, Yellow crystalline powder
Molecular formula	$C_{15}H_{10}O_7$
Molecular weight (g mol^{-1})	302.236
Melting point (°C)	316°
Partition coefficient (Log P)	1.48
Water solubility (µg/mL)	0.4 ± 0.05
BCS Class	Class IV drug

Calibration Profile of QCN

The UV-Vis analysis starts by performing the QCN (1 µg/mL) solution in the region of 200 to 800 nm for the determination of the drug's maximum absorbance. The required amount of QCN stock solution was taken into 5 mL volumetric flasks, and the flask was made up to 5 mL with ethanol to set final concentrations ranging from 0.1-0.5 µg/mL. The solutions were properly mixed and their absorbances were measured on a UV-Vis spectrophotometer (Shimadzu, Japan, UV-2450) at λ_{max} 369 nm with ethanol solvent as a reference, and the calibration curve was drawn (displayed in Figure 2.5). Linearity parameters of calibration curve for QCN drug are shown in Table.2.6.

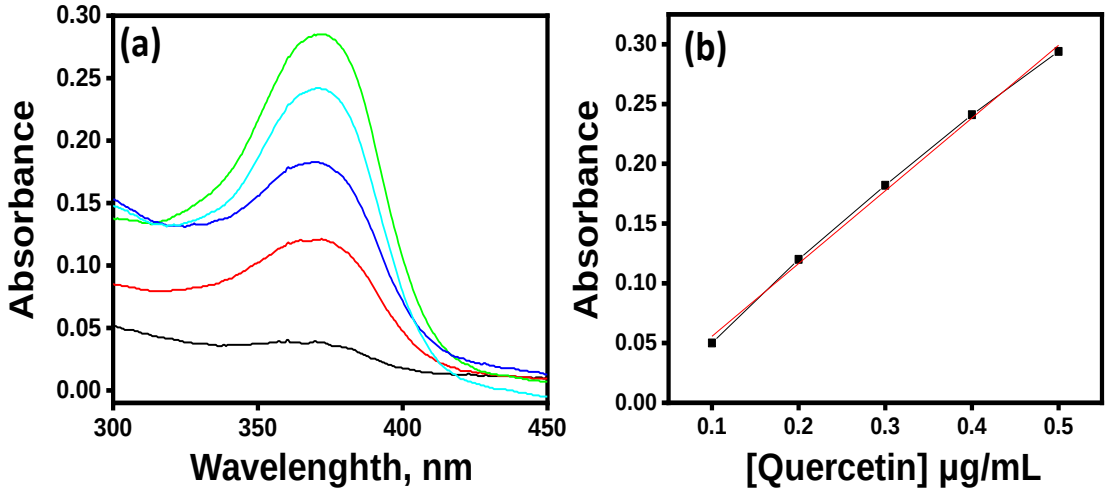

Figure 2.5: (a) UV-Vis graph and (b) Calibration curve of QCN drug.

Table .2.6: Statistical analysis parameters for calibration curve of QCN drug in ethanol.

Regression equation	y = a+bx
Intercept	-0.0053 ± 0.00603
Slope	0.609 ± 0.01818
Pearson's r	0.9986
Correlation coefficient (R^2)	0.9973
Adjusted R^2	0.9964

2.1.3.2: Curcumin

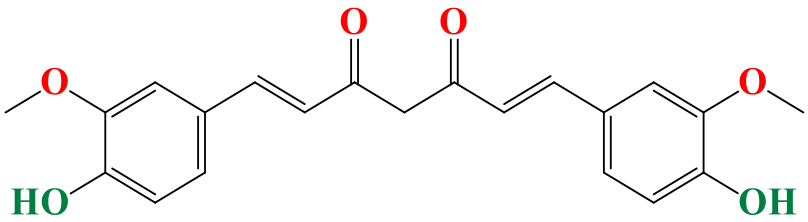

Figure 2.6*:* Molecular structure of CUR

Natural plant products have been used in a wide range of complementary and alternative medicine (CMA) therapies and diagnostic studies. Natural products have the advantage of being effective and benign, and they can be administered at therapeutic dosages much lower than their toxic levels. The solid gold of India, turmeric is a natural flowering plant belonging to the perennial herb family, Curcuma longa. CUR, a polyphenol taken from the herb Curcuma longa's rhizome, exhibits a variety of biological and pharmacological activities.

CUR is a diarylheptanoid comprised of two aromatic rings joined by a seven-carbon chain. It contains two ortho-methoxy phenol groups, two enone groups, and a keto-enol moiety, among other functionally active groups (Figure 2.6). On the Asian continent and specifically India, CUR has been operated for a period of years to cure several disorders due to its antioxidant, anti-inflammatory, antiseptic, antimicrobial, anticoagulant, wound healing, and anticarcinogenic properties[12,13].

The general properties of CUR are shown in Table 2.7.

- CUR was obtained from Sigma-Aldrich (St.Luice, MO, USA).

Table.2.7: General properties of CUR.

Physical state	Solid, Bright yellow powder
Molecular formula	$C_{21}H_{20}O_6$
Molecular weight (g mol^{-1})	368.38
Melting point (°C)	183°
Partition coefficient (Log P)	~3
Water Solubility (ng/mL)	11 ± 0.02
BCS Class	Class IV drug

Calibration Profile of CUR

The UV-Vis analysis starts by performing the CUR (1 µg/mL) solution in the region of 200 to 800 nm for the determination of the drug's maximum absorbance. The required amount of CUR stock solution was taken into 5 mL volumetric flasks, and the flask was made up to 5 mL with ethanol to set final concentrations ranging from 0.1-0.5 µg/mL. The solutions were properly mixed and their absorbances were measured on a UV-Vis spectrophotometer (Shimadzu, Japan, UV-2450) at λ_{max} 425 nm with ethanol solvent as a reference, and the calibration curve was drawn (displayed in Figure 2.7). Linearity parameters of calibration curve for CUR drug are shown in Table.2.8.

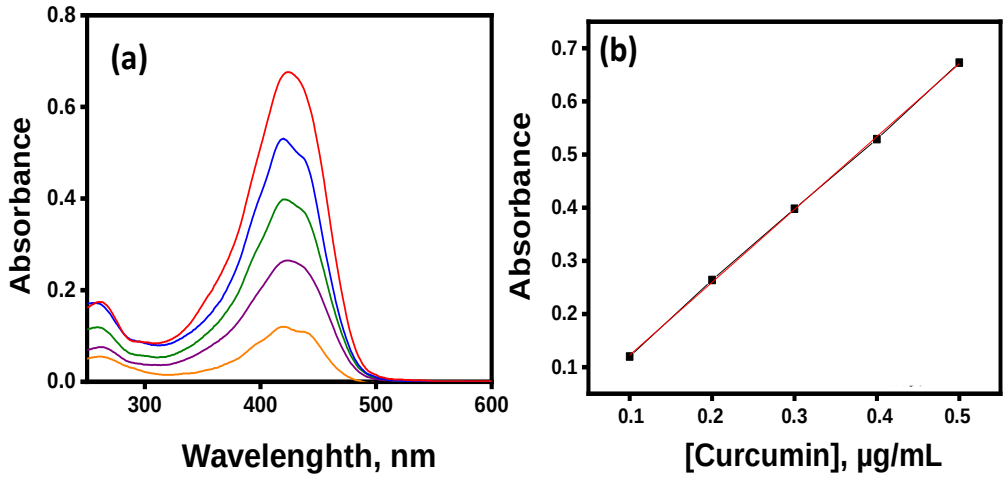

Figure 2.7: (a) UV-Vis graph and (b) Calibration curve of CUR drug.

Table .2.8: Statistical analysis parameters for calibration curve of CUR drug in ethanol.

Regression equation	y = a+bx
Intercept	-0.0145 ± 0.0044
Slope	0.1371 ± 0.00135
Pearson's r	0.9998
Correlation coefficient (R^2)	0.9997
Adjusted R^2	0.9996

2.1.3.3: Glipizide

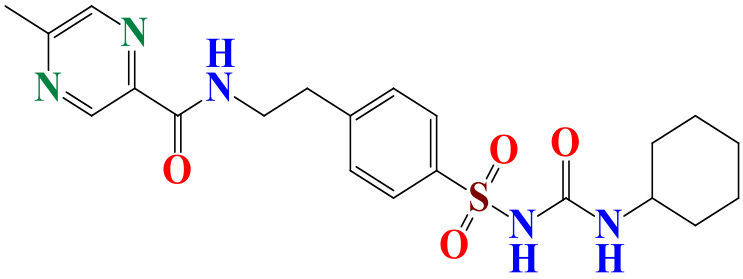

Figure 2.8: Molecular structure of GLN

GLN is a BCS Class-II hypoglycemic agent and is generally prescribed for the treatment of type 2 diabetes mellitus patients [14,15]. It is an acidic drug with a low pKa (pKa = 5.9) that is practically insoluble in water and acidic environments [16]. When it is supplied orally, its absorption is inconsistent in the patients (diabetic), due to the weak gastric transportability and/or gastric emptying. Such inconsistent absorption of GLN is pharmacologically relevant, as its efficacy is absorption rate dependent. Also, GLN absorption from the GI fluids is limited due to its poor aqueous solubility.

The general properties of GLN are shown in Table 2.9.

- GLN was a gift sample from local pharmaceutical industry (Vadodara, India).

Table.2.9: General properties of GLN.

Physical state	Solid, White powder
Molecular formula	$C_{21}H_{27}N_5O_4S$
Molecular weight (g mol^{-1})	445.53
Melting point (°C)	208°
Partition coefficient (Log P)	~1.9
Water Solbility (mg/mL)	0.0335±0.0021
BCS Class	Class II drug

Calibration Profile of GLN

The UV-Vis analysis starts by performing the GLN (1 µg/mL) solution in the region of 200 to 800 nm for the determination of the drug's maximum absorbance. The required amount of GLN stock solution was taken into 5 mL volumetric flasks, and the flask was made up to 5 mL with ethanol to set final concentrations ranging from 10-50 µg/mL. The solutions were properly mixed and their absorbance were measured on a UV-Vis spectrophotometer (Shimadzu, Japan, UV-2450) at λ_{max} 275 nm with DMSO solvent as a reference, and the calibration curve was drawn (displayed in Figure 2.9). Linearity parameters of calibration curve for GLN drug are shown in Table.2.10.

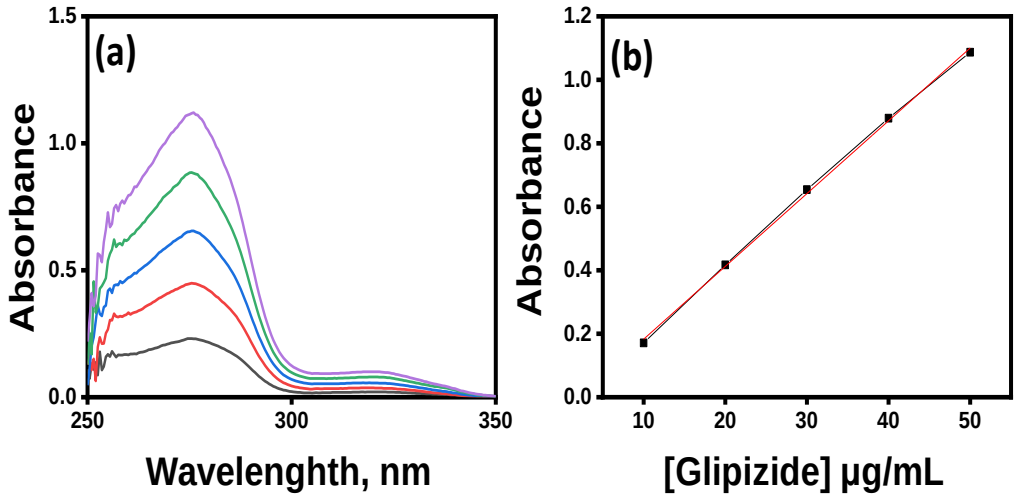

Figure 2.9: (a) UV-Vis graph and (b) Calibration curve of GLN drug.

Table 2.10: Statistical analysis Parameters for calibration curve of GLN drug in DMSO

Regression equation	y = a+bx
Intercept	-0.0466 ± 0.014
Slope	0.0229 ± 0.00431
Pearson's r	0.9994
Correlation coefficient (R^2)	0.9989
Adjusted R^2	0.9985

2.1.4: Other materials used in biological investigations

- The dialysis membrane bag for the in-vitro drug release study was bought from HiMedia (India). It had an average flat width of 31.13 mm, an average diameter of 21.5 mm, and a molecular weight of 12 kDa–14 kDa.
- Nutrient agar (sterile) and agar culture media were obtained from HiMedia (India) for the antimicrobial study.
- DMEM, FBS, and the antibiotic mixture PSN were purchased from Invitrogen (USA) for antimicrobial analysis.
- Cell culture-grade DMSO, MTT, and Trypan blue dye were purchased from Sigma-Aldrich (USA) for cell viability and proliferation measurements for the anti-carcinogenic study.
- A human breast adenocarcinoma (MCF-7) cell line was obtained from the National Center for Cell Science (NCCS), Pune, Maharashtra (India), for an anti-carcinogenic study.
- All other analytical-grade chemicals used were purchased from Merck (Germany).

2.2: Experimental Design

The purposes of optimization approaches are to maintain public and industrial quality, economy, and safety. Assembling pharmaceutical product is a complex procedure and usually requires various materials and methods of preparation. Moreover, its commercialization is challenging due to a lack of scale-up data and regulatory issues. Apart from these development issues, inadequate guidelines on shelf-life, bioavailability, and impurities are barriers to commercialization and need formulation novelty. The QbD is the latest trend to develop and optimize various significant pharmaceutical processes. According to QbD, quality should build into products rather than only be assessed after manufacturing. Applying QbD principles in pharmaceutical product is expected to help overcome existing issues with providing wider regulatory acceptance, and accelerate clinical application.

Whereas the importance of optimizing a pharmaceutical product required the identification of essential factors involved, a more cost-effective and efficient method of formulating the product, and enhancing the consistency and effectiveness of quality specifications in the formulation. For this we use D-Optimal Design and Central Composite Design as optimization tools in the present research work. Both designs were created operating the Design Expert® software (version 7.0.) developed by Stat Ease Inc. (USA).

2.2.1: D-optimal Design

Medicinal formulation development should concurrently utilize a number of preformulation parameters. The consequences of the independent variables are excluded in the usual optimization approach. The complexities of recognizing the true interaction between dependent and independent responses create issues in pharmaceutical formulation optimization. D-optimal design, a subset of experimental design, is the widely used RSM for optimizing formulation attributes, and it has been utilized to optimize pharmaceutical formulation. A three-level D-optimal design was used to optimize the formulation attributes of pharmaceutical formulations with the principal goal of understanding the relationships between dependent variable and independent variables. The, D-optimal design in combination with Response surface methodology, is a systematic way of designing, optimizing, and delivering any active pharmaceutical substance or process. The D-optimal design is a fast method for finding the impact of independent variables on each dependent

variable. The optimal formulation has been determined using ANOVA regression analysis[17].

- When more than three factors are selected, the D-optimal design has very few runs in comparison to other optimization designs. Hence, this design required a smaller number of set-up measurements and also permitted the inclusion of the combined mixture and process variables in the same experimental design.
- The The main advantages of D-optimal design are that it is not simple and is also irregular, which gives it more precise values. Such concentrations are easily manageable in the case of Pluronic mixtures.

The D-optimal design tool was used to optimize the Pluronic-based mixed micelles PFPC, and CUR-PFPC was composed using the Pluronic P123, Pluronic F68, and PC.

2.2.2: Central Composite Design(CCD)

An experimental design known as the CCD concept developed during the process of optimizing and selecting the best potential product from ongoing batches. The CCD model is a key component of RSM. The most significant benefit of this form of optimization model is that it is more precise, and there is no need for a three-level factorial experiment to develop a second-order quadratic model. The CCD was used to determine the impact of two independent variable on dependent variable using the principal of design of experiments. After extracting the CCD model from the experiment, a linear regression model was used to generate the model, and coded data were employed. [18].

CCD is used for the optimization of micellar formulation for the following reason:

- This technique well estimates the 1^{st} and 2^{nd} order kinetics.
- It is designed to provide accurate estimates for a quadratic model as well as sequential experiments.
- CCD is a two-level factorial design that is also augmented with centre points and axial points.
- In CCD, five levels are required for each factor (this number of levels can be minimized through proper selection of $\alpha=1$). In CCD, when star points serve as the centre point for each face of the factorial space, only three levels of each variable are required.

- CCD gives better prediction capability near the centre point of the design space, which is very helpful for formulations.

The CCD tool was used to optimize the mixed Pluronic micellar systems formulated using the functionalized Pluronic SA-F127 and biocompatible TPGS for the bioavailability of the GLN drug.

2.3: Characterization methods

2.3.1: Determination of critical micelle concentration

Pyrene is hydrophobic and has a low solubility in water, but it has a greater solubility in a micellar environment. When the polymer concentration is less than CMC, the absorbance differs slightly, and it changes notably when it attains CMC. The reason for this is that pyrene can move from the water phase into the micelles once the micelles have formed. This changes the polarity around the micelles.

2.3.1.1: CMC using UV-Vis Spectroscopy

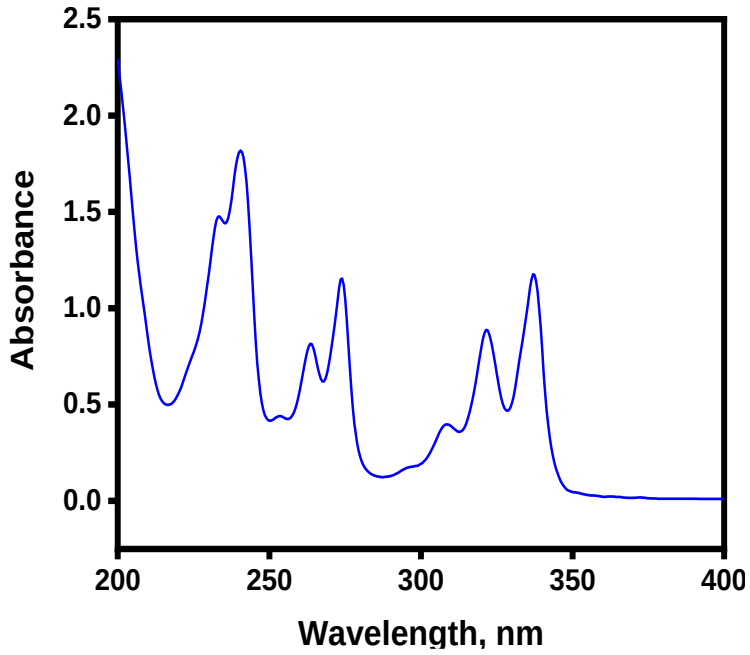

Figure 2.10: UV-vis spectrum of pyrene

The CMCs of mixed Pluronic polymer solutions were determined using the pyrene UV probe method with the required modification at 30°±1°C [19]. The simple absorbance spectra of pyrene in ethanol are shown in Figure 2.10. The five prominent pyrene peaks at 240, 260, 272, 320, and 335 nm are easily seen in the spectrum because of the presence of multiple concentric rings.

The concentrations of Pluronic sample solutions ranging from 0.0001 %w/v to 1 %w/v were prepared with the appropriate dilution using water. An aliquot of 50µl fixed

amount of 1×10^{-4}M of pyrene was added to each prepared sample. Before measurement, the Pluronic sample solution was placed for 24 hrs under dark conditions. The sample solutions were properly filtered through a 0.45µm filter, and the absorbance was determined using a UV–Visible spectrophotometer. The plot of intensity ratio (chosen here as I_1/I_3) against Log Pluronic concentration of sample solutions was used to determine the CMC.

2.3.1.2: CMC using Fluorescence Spectroscopy

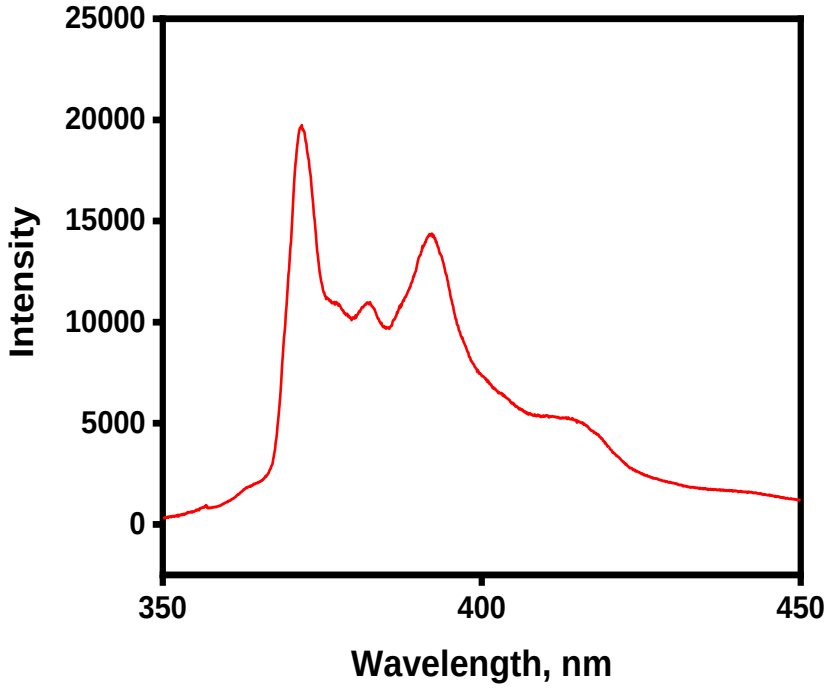

Figure 2.11: Fluorescence spectrum of pyrene

The CMC of the Pluronic sample solutions were determined using a fluorescence spectrofluorometer (RF-6000, Shimadzu) equipped with thermostatic bath at 30°±0.5°C with a pyrene as a probe. Figure 2.11 shows the simple fluorescence spectra of pyrene. Sample solutions were added with a series of dilutions into preplanned dry pyrene, and the pyrene concentration was kept constant (6.0×10^{-7}M) in each of the sample solutions. The mixtures were incubated overnight in the dark at ambient temperature. Analysis was done at a fixed excitation wavelength of 335 nm using constant slit widths of 3 nm for excitation and 3 nm for emission. Spectrum ranging from 350 nm-450 nm were scanned at a rate of 60 nm/min. Pyrene has been applied, and the intensities ratio of the first (I_1=372) and third(I_3=383)

vibronic peaks; (I_1/I_3) are usually taken to find the polarity level of its environment. CMC is calculated using a plot of the intensities ratio of the first and third vibronic peaks (I_1/I_3) vs. concentration of samples (using Boltzmann sigmoidal fitting) [20]. The inflection point of the plot of I_1/I_3 against Log Pluronic concentration of sample solutions is taken as the CMC of system.

2.3.2: CPT measurements

The CPT measurements of samples were conducted by submerging closed glass tubes that contained each solution (1.0 %w/v) in a water bath at RT. The temperature was then increased gradually from RT at a rate of 1°C/min with proper stirring using a magnetic stirrer with temperature control. The CPT was determined by the visual appearance of solutions from clear to turbid [21]. After the temperature exceeded the CPT, the system was cooled down, and the whole process was repeated to check the measurements' reproducibility. The maximum uncertainty in the CPT measurement was ±0.5ºC.

2.3.3: Drug solubility determinations

Drug solubility measurements were performed using a UV-Visible spectrophotometer. The studies of solubilization in systems were performed by adding the excess drug in sample solutions. After equilibrium, the residual non-solubilized drug was removed by centrifugation and filtration through a 0.45 µm syringe filter membrane. After appropriate dilution, the soluble amount of the drug was finding out by analyzing absorbance at the specific λ_{max}, and absorbance was fitted with a standard calibration curve prepared in suitable solvent to find concentration and solubility. The experiment was done thrice, and the results were shown as the mean of the three.

After the measurement, the % drug loading and % encapsulation efficiency of the drug in Pluronic micellar formulations were calculated using equations (1) and (2).

$$\%\mathrm{DL} = \frac{\text{Amount of drug in micelles}}{\text{Amount of total polymers}} \times 100 \ldots (1)$$

$$\%\ \mathrm{EE} = \frac{\text{Amount of drug micelles}}{\text{Amount of drug used}} \times 10 \ldots (2)$$

2.3.4. Structural characterization methods

2.3.4.1: DLS analysis

DLS measures the temporal fluctuations of the light scattered due to the brownian motion of the particles, when a solution containing the particles is placed in the path of a monochromatic beam of light. It gives particle size information in terms of hydrodynamic diameter (Dh) along with the PDI of the sample. DLS is a sensitive, disruptive, and impressive analytical tool regularly used for the characterization of polymers and colloids in solution. It has also been employed to measure the size and size distribution profile of nanoparticles/nanomicelles. DLS is also known as photon correlation spectroscopy (PCS) or quasi-elastic light scattering (QELS).

The DLS measurements utilize scattering angles of 90° or 173° using a He–Ne laser as a source of light, that is, detector position at a back angle 173° and right angle 90° to incident light [22]. Brownian motion of individual particles is converted into particle size, which is calculated by software using the well-known Stokes–Einstein equation.

$$D = \frac{kT}{6\pi\eta R} \qquad \text{…..(3)}$$

Here, D is diffusion coefficient, k is Boltzmann's constant, T is temperature, η is viscosity of solvent, and R_h is the rheodynamic radius of particle solution [23].

For D_h measurements, after proper dilution of Pluronic micellar formulations with a solvent to avoid multiple scattering factors filled in a cylindrical cuvette and placed in Zetasizer Nano-ZSP instrument (Malvern, UK) outfitted with Nano ZS® software for data requisition and analysis. All the DLS experiments were performed in triplicate to get mean value±SD.

2.3.4.2: SEM measurements

SEM is the high-resolution electron microscopy technique for the visualization and characterization of surfaces. In opposite to optical microscopy, which utilizes a light source and glass lenses to illuminate specimens to generate magnified images, SEM employs accelerated electrons beams and electromagnetic lenses to generate images of much higher resolution based on the shorter wavelengths of electrons than visible light photons. In SEM,

the electrons are located and scanned sequentially across the specimen. At every location, signals are emitted from the sample specimen and collected through detectors. The detector signal is synchronized with standard location of the electron beam on the specimen, and the signal intensity is utilized to modulate the corresponding image pixel. These signals are combined to form an image.

This surface-imaging technique is totally able to measure size, size distribution, formation, and morphology of the nano-materials.

The micellar sample for morphological analysis was prepared by air-drying a drop of micellar suspension on a SEM sample holder. The surface morphology was examined using a conventional SEM (JEOL, JSM-5610LV, Japan)

2.3.4.3: TEM analysis

TEM is another useful electron microscopy technique of characterization of nanoscale materials. Likewise SEM, it also works with accelerated electrons beams and electromagnetic lenses to generate images. Many disadvantages of SEM regarding the better spatial resolution are fulfilled by using TEM. It gives a notable enhanced resolution (0.0001 μm), about 1 to 2 orders of magnitude higher than that of the SEM. It is a quantitative method to determine the particle size, shape and distribution. It shows the direct imaging of the material at the atomic scale. TEM is routinely used in the morphological analysis of polymeric micelles with special sample preparation method.

A TEM instrument analyzed the morphological examination of the samples prepared under the specific condition worked at an accelerating 200 kV (Jeol, Japan). First, a 5 μL sample's dispersion was layered on the carbon-coated copper metal grid (200 meshes) and negatively stained with one drop of freshly prepared 2% aqueous solution of uranyl acetate. The grid was kept for drying at RT and for contrast enhancement, and then the sample was observed by TEM and photographed with a digital camera.

2.3.4.4: SANS analysis

"The SANS experiments were made using an Indian-built SANS tool at the BARC in Mumbai, Maharashtra, India. The mean incident neutron beam wavelength with a resolution ($\Delta\lambda/\lambda$) of about 10% was 5.2 Å. A linear position-sensitive detector was employed to find for scattered neutrons in an angular 0.5–15° range. The scattering vectors 'Q' in the range of

0.015–0.3 Å^{-1} of scattered neutrons were observed. The samples prepared in D_2O and were measured using a 5 mm thick quartz holder. The data was normalized to the cross-sectional unit. For the background and solvent contribution, all SANS distributions were precisely calculated. The empty cell contribution, the transmission data, and solvent contribution were normalized to the cross-sectional unit and presented on an absolute scale with standard protocols. Various characteristics of micelles were investigated in the analysis.

The differential scattering cross-section per unit volume ($d\Sigma/d\Omega$) as measured for a system of monodisperse particles in a medium can be expressed as

$$\left(\frac{d\Sigma}{d\Omega}\right)(Q) = nV^2(\rho_p - \rho_s)^2 P(Q)S(Q) + B \ , \qquad \ldots (4)$$

where n denotes the number density of particles. $P(Q)$ is the intraparticle structure factor and $S(Q)$ is the interparticle structure factor. B representing incoherent background, which is mainly due to the hydrogen present in the sample. Intraparticle structure factor $P(Q)$ is decided by the shape and size of the particle and is the square of single-particle form factor $F(Q)$. For a spherical particle of radius R, $P(Q)$ is given by

$$P_p(Q) = 9\left[\frac{\sin(QR) - QR\cos(QR)}{(QR)^3}\right]^2 . \qquad \ldots (5)$$

$\rho_p$and ρ_s are, respectively, the scattering length densities of particle and solvent and $V$is the volume of the particle.

The form factor of the micelles comprises four terms: the self-correlation of the core, the self-correlation of the chains, the cross term between core and chains, and the cross term between different chains. It is given by

$$P_m(Q) = N_s^2 P_s(Q) + 2N_s P_c(Q) + 2N_s(2N_s - 1)P_{cc}(Q) + 4N_s^2 P_{sc}(Q) \qquad \ldots (6)$$

where N_s is the aggregation number of the micelles. The subscript s (= core) and c (= chain) are used here.

At higher concentrations, an interaction between micelles takes place and a peak arising from the structure factor, $S(Q, R_{hs}, \phi)$ where R_{hs} is hard sphere radius and ϕ is volume fraction of micelles, appears in the scattering intensity. $S(Q)$ describes the interaction between the particles present in the system and depends on the spatial distribution of micelles, is given by

$$S(Q) = 1 + 4\pi n \int (g(r) - 1) \frac{\sin(Qr)}{Qr} r^2 dr \quad , \qquad \ldots (7)$$

where $g(r)$ is the radial distribution function describing the arrangement of the micelles. In the case of Pluronic micelles, the interparticle interaction (direct correlation between two scattering objects) is obtained using Ornstein–Zernike equation with the Percus-Yevick approximation and employing hard sphere potential between micelles, and the analytical form of the structure factor is given as

$$S(Q) = \frac{1}{1 + 24\phi \ (G(x)/x)} \quad , \qquad \ldots (8)$$

where R_{hs} is the hard sphere micellar radius consisting of both the core and the shell which gives the physical size of the micelle, ϕ is the hard sphere volume fraction of the micelles in the solution, and G is a function of $x = 2QR_{hs}$ and ϕ.

In this equation, $G(x)$ is further defined as follows:

$$G(x) = \frac{\alpha(\phi)}{x^2}(\sin x - x\cos x) + \frac{\beta(\phi)}{x^3}[2x\sin x + (2 - x^2)\cos x - 2] + \frac{\gamma(\phi)}{x^5}[-x^4\cos x + 4\{(3x^2 - 6)\cos x + (x^3 - 6x)\sin x + 6)\}] \qquad \ldots (9)$$

where

$$\alpha(\phi) = (1 + 2\phi)^2 / (1 - \phi)^4$$

$$\beta(\phi) = -6\phi(1 + \frac{\phi}{2})^2 / (1 - \phi)^2$$

$$\gamma(\phi) = \frac{\phi\alpha}{2} \qquad \ldots (10)$$

In fitting the experimental scattering data, three unknown parameters, R_c, R_{hs} and ϕ have been considered as fitting parameters in the analysis. The aggregation number of micelles, N_{agg} can be calculated using the expression, $N_{agg} = V_m/V_h$ where V_m (= 4/3 πR_c^3) is the micellar volume and V_h is the volume of the hydrophobic part of the surfactant monomer.

The polydispersity in size distribution of particle is incorporated using the following integration

$$\frac{d\Sigma}{d\Omega}(Q) = \int \frac{d\Sigma}{d\Omega}(Q,R) f(R) dR + B \,, \qquad \ldots (11)$$

where $f(R)$ is the particle size distribution and usually accounted by a log-normal distribution as given by

$$f(R) = \frac{1}{\sqrt{2\pi} R\sigma} \exp\left[-\frac{1}{2\sigma^2} \left(\ln \frac{R}{R_{med}} \right)^2 \right], \qquad \ldots (12)$$

where R_{med} is the median value and $\sigma$is the standard deviation (polydispersity) of the distribution. The mean radius (R_m) is given by $R_m = R_{med} \exp(\sigma^2/2)$.

The data have been analyzed by comparing the scattering from different models to the experimental data.**"** The above-quoted theory of SANS analysis is known in the scientific community and refers to Aswal et al. [24] and Shaikh et al. [25].

2.3.4.5: Rheology/Viscosity measurements

The rheology study focuses on the study of how matter can be deformed and moved. When using rheology to describe a material, it is important to consider both the material's viscosity and the shear-induced yield stress. The rheological characterization of compounds provides a comprehensive overview of the viscoelastic flow behavior of the materials. It is very important to every material because rheological responses are closely related to the system's final structures.

Rheological studies were investigated using rheometer (HAAKE, Thermo Fisher, USA) using parallel plate geometry (PP 25 CS L) attached with temperature control device (MTMC MARS III). The shear-rate was ranged from 0.1 to 200 S^{-1}. The measurements were carried out at 30±0.5°C.

2.3.5 Solid state characterization methods

2.3.5.1: FTIR measurements

Fourier transform infrared (FTIR) spectroscopy is widely used for the identification of materials in films and provides information on the interaction mechanisms of analytes of interest and molecular organization.

The FTIR spectrums of samples were measured using an IR spectrophotometer (Shimadzu, Japan) using the KBr pellet method with a better 4 cm^{-1} resolution. The samples were scanned in the wavenumber range of 4000 cm^{-1} - 500 cm^{-1} at RT and determined the various bands of different functional groups to identify drug-polymer interaction.

2.3.5.2: XRD analysis

X-ray diffraction is a useful technique for determining the physicochemical characteristics or crystalline nature of a sample. It is used to identify the arrangement of atoms within macroscopic entities like macromolecules and inorganic compounds.

To detect the crystalline or amorphous state of the samples, a powder X-ray diffractometer (Phillips X-Pert MPD, USA) operating at 40 kV/40 mA was used. Each sample was estimated in transmission mode from 2°-50° ranges of 2θ diffraction angles with a scanning speed of 0.5°/s and a 1 second dwell time between each step.

2.3.5.3: DSC analysis

Various methods are used to characterize nanomaterials. Among them, thermal analysis methods are those in which a physical property of a compound or its reaction products is measured as a function of temperature. DSC is the most often employed thermal analysis method, mainly due to its speed, simplicity, and easy availability. DSC is a quantitative technique and measures the difference in the heat flow between the sample and the reference. DSC provides qualitative and quantitative information to the thermal properties of solid materials such as the melting and degradation temperatures, glass transition temperature, melt and crystallization enthalpy, specific and latent heats, polymorphism, and purity of the materials

DSC (60 plus, Shimadzu, Japan) of samples were examined. Samples (5 mg-6 mg) were taken in aluminum pans and controlled heating with 10°C/min rate using the inert nitrogen atmosphere at a temperature range of 25°C–300°C with a flow rate (100 mL/min). The internal standard was aluminum oxide.

2.3.5.4: NMR Spectroscopy

The NMR method is an effective strategy that contributes significantly to a better understanding of the nucleus-level site of drug solubilization in micelles. NMR spectroscopy

is used to learn more about how the amount of drug entrapped in micelles and how well they trap drugs affects their mechanical properties, which in turn may affect how they behave in a biological medium.

To confirm the location of the drug in the system, ^{1}H-NMR spectra were recorded on a Bruker-III HD 500 MHz spectrometer. The pure drug was dissolved in deuterated chloroform ($CDCl_3$). The micellar solutions were prepared in deuterated water (D_2O). The ^{1}H-NMR spectra were recorded with 32 scans.

2.3.5.5: Stability Study

The stability study of formulation was performed as per ICH guidelines. The formulation was stored at RT and determined the drug content for fixed time point (pre-decided) using UV-Vis spectroscopy. The stability study was also determine by checking the increase or decrease in particle size at RT and refrigerated condition (2°C–4°C) using the DLS technique. Each measurement was performed in triplicate.

2.3.6: Biological Investigations

- The *in-vitro* drug release studies were investigated using the dialysis bag method.
- The antioxidant activities of pure drug and drug loaded mixed Pluronic micellar solutions were measured by their ability to scavenge the DPPH radicals.
- *In-vitro* cell proliferation activity studies were determined by the MTT assay method.
- *In-vitro* cell viability activity studies were determined by the Trypan blue assay method.
- *In-vitro* antimicrobial (antibacterial/antifungal) activity was carried- out using the agar well diffusion technique.
- *Ex-vivo* drug permeability studies were done by Franz diffusion cell using isolated goat intestine segments.
- *In-vivo anti-diabetic study by measuring* the glucose level of the blood using an Accu-Chek glucometer in normal healthy male Wistar rats.

The detail procedure of the above-mentioned biological investigations is shown in the respective chapters where it was used.

2.4. References

[1] A. V Kabanov, E. V Batrakova, V.Y. Alakhov, Pluronic® block copolymers as novel polymer therapeutics for drug and gene delivery, J. Control. Release. 82 (2002) 189–212.

[2] P. Holmqvist, P. Alexandridis, B. Lindman, Modification of the microstructure in poloxamer block copolymer-water-"oil" systems by varying the "oil" type, Macromolecules. 30 (1997) 6788–6797.

[3] R.L. Duan, X. Sun, J. Liu, T. Gong, Z.R. Zhang, Mixed micelles loaded with silybin-polyene phosphatidylcholine complex improve drug solubility, Acta Pharmacol. Sin. 32 (2011) 108–115.

[4] K.K. Ajeeshkumar, P.A. Aneesh, N. Raju, M. Suseela, C.N. Ravishankar, S. Benjakul, Advancements in liposome technology: Preparation techniques and applications in food, functional foods, and bioactive delivery: A review, Compr. Rev. Food Sci. Food Saf. 20 (2021) 1280–1306.

[5] M.T. Luiz, L.D. Di Filippo, R.C. Alves, V.H.S. Araújo, J.L. Duarte, J.M. Marchetti, M. Chorilli, The use of TPGS in drug delivery systems to overcome biological barriers, Eur. Polym. J. 142 (2021) 110129.

[6] S. Rathod, P. Bahadur, S. Tiwari, Nanocarriers based on vitamin E-TPGS: Design principle and molecular insights into improving the efficacy of anticancer drugs, Int. J. Pharm. 592 (2021) 120045.

[7] A. Mahajan, S. Kaur, S. Kaur, Design, formulation, and characterization of stearic acid-based solid lipid nanoparticles of candesartan cilexetil to augment its oral bioavailability, Asian J Pharm Clin Res. 11 (2018) 344–350.

[8] C. Bronner, Y. Landry, Kinetics of the inhibitory effect of flavonoids on histamine secretion from mast cells, Agents Actions. 16 (1985) 147–151.

[9] T.N. Kaul, E. Middleton Jr, P.L. Ogra, Antiviral effect of flavonoids on human viruses, J. Med. Virol. 15 (1985) 71–79.

[10] M. Fiorani, R. de Sanctis, P. Menghinello, L. Cucchiarini, B. Cellini, M. Dachà, Quercetin prevents glutathione depletion induced by dehydroascorbic acid in rabbit red blood cells, Free Radic. Res. 34 (2001) 639–648.

[11] T. Pralhad, K. Rajendrakumar, Study of freeze-dried quercetin–cyclodextrin binary

systems by DSC, FT-IR, X-ray diffraction and SEM analysis, J. Pharm. Biomed. Anal. 34 (2004) 333–339.

[12] K. Morshedi, S. Borran, M.S. Ebrahimi, M.J. Masoud khooy, Z.S. Seyedi, A. Amiri, M. Abbasi-Kolli, M. Fallah, H. Khan, A. Sahebkar, Therapeutic effect of curcumin in gastrointestinal cancers: A comprehensive review, Phyther. Res. 35 (2021) 4834–4897.

[13] M. Rai, A.P. Ingle, R. Pandit, P. Paralikar, N. Anasane, C.A. Dos Santos, Curcumin and curcumin-loaded nanoparticles: antipathogenic and antiparasitic activities, Expert Rev. Anti. Infect. Ther. 18 (2020) 367–379.

[14] G. Bruni, I. Ghione, V. Berbenni, A. Cardini, D. Capsoni, A. Girella, C. Milanese, A. Marini, The Physico-Chemical Properties of Glipizide: New Findings, Molecules. 26 (2021) 3142.

[15] J. Joya-Galeana, M. Fernandez, A. Cervera, S. Reyna, S. Ghosh, C. Triplitt, N. Musi, R.A. DeFronzo, E. Cersosimo, Effects of insulin and oral anti-diabetic agents on glucose metabolism, vascular dysfunction and skeletal muscle inflammation in type 2 diabetic subjects, Diabetes. Metab. Res. Rev. 27 (2011) 373–382.

[16] R.K. Verma, S. Garg, Selection of excipients for extended release formulations of glipizide through drug–excipient compatibility testing, J. Pharm. Biomed. Anal. 38 (2005) 633–644.

[17] N.-K. Nguyen, A.J. Miller, A review of some exchange algorithms for constructing discrete D-optimal designs, Comput. Stat. Data Anal. 14 (1992) 489–498.

[18] S. Bhattacharya, Central Composite Design for Response Surface Methodology and Its Application in Pharmacy, in: P. Kayaroganam (Ed.), IntechOpen, Rijeka, 5 (2021) 95835.

[19] R.K. Sharma, S. Shaikh, D. Ray, V.K. Aswal, Binary mixed micellar systems of PEO-PPO-PEO block copolymers for lamotrigine solubilization: a comparative study with hydrophobic and hydrophilic copolymer, J. Polym. Res. 25 (2018) 1–11.

[20] J.K. Salem, I.M. El-Nahhal, S.F. Salama, Determination of the critical micelle concentration by absorbance and fluorescence techniques using fluorescein probe, Chem. Phys. Lett. 730 (2019) 445–450.

[21] D. Nandni, K.K. Vohra, R.K. Mahajan, Study of micellar and phase separation

behavior of mixed systems of triblock polymers, J. Colloid Interface Sci. 338 (2009) 420–427.

[22] P.C. Griffiths, B. Cattoz, M.S. Ibrahim, J.C. Anuonye, Probing the interaction of nanoparticles with mucin for drug delivery applications using dynamic light scattering, Eur. J. Pharm. Biopharm. 97 (2015) 218–222.

[23] C.M. Hoo, N. Starostin, P. West, M.L. Mecartney, A comparison of atomic force microscopy (AFM) and dynamic light scattering (DLS) methods to characterize nanoparticle size distributions, J. Nanoparticle Res. 10 (2008) 89–96.

[24] V.K. Aswal, P.S. Goyal, Small-angle neutron scattering diffractometer at Dhruva reactor, Curr. Sci. 79 (2000) 947–953.

[25] S.J. Shaikh, Self-assembly of block copolymeric systems: Design and drug delivery Perspectives, Maharaja Sayajirao University of Baroda (India) PP - India, (2019).